34th Annual International Conference of the IEEE EMBS
San Diego, California USA, 28 August - 1 September, 2012

Validation of Accuracy of Liver Model with Temperature-Dependent Thermal Conductivity by Comparing the Simulation and in vitro RF Ablation Experiment

Hiroki Watanabe, Nozomu Yamazaki, Yosuke Isobe, XiaoWei Lu, Yo Kobayashi, Tomoyuki Miyashita, Takeshi Ohdaira, Makoto Hashizume, and Masakatsu G. Fujie, *Fellow*, *IEEE*

Abstract — **Radiofrequency (RF) ablation is increasingly used to treat cancer because it is minimally invasive. However, it is difficult for operators to control precisely the formation of coagulation zones because of the inadequacies of imaging modalities. To overcome this limitation, we previously proposed a model-based robotic ablation system that can create the required size and shape of coagulation zone based on the dimensions of the tumor. At the heart of such a robotic system is a precise temperature distribution simulator for RF ablation. In this article, we evaluated the simulation accuracy of two numerical simulation liver models, one using a constant thermal conductivity value and the other using temperature-dependent thermal conductivity values, compared with temperatures obtained using in vitro experiments. The liver model that reflected the temperature dependence of thermal conductivity did not result in a large increase of simulation accuracy compared with the temperature-independent model in the temperature range achieved during clinical RF ablation.**

I. Introduction

Radiofrequency (RF) ablation is an important method for treating liver tumors and has been increasing use in recent years. RF ablation involves percutaneous introduction of an electrode into the tumor and application of RF energy, thereby increasing the temperature of the tissue via ionic agitation generated by the microwaves. Tissue coagulation occurs when the tissue around the electrode reaches a temperature of ~60°C. Moisture evaporation then occurs and the tissue becomes completely necrotic at about 90°C. This percutaneous procedure offers proven effectiveness and safety and has the added advantage of being minimally invasive.

Manuscript received April 15, 2012. This work was supported in part by the Global COE (Centers of Excellence) Program "Global Robot Academia," in part by "High-Tech Research Center" Project for Private Universities: matching fund subsidy from MEXT (the Ministry of Education, Culture, Sports, Science and Technology of Japan), in part by a Grant for Scientific Research (B) (22360108), and a Grant for Scientific Research (A) (23240081) from the MEXT.

H. Watanabe, Y. Kobayashi, T. Miyashita, M. G. Fujie, Members of the Faculty of Science and Engineering, Graduate School of Science and Engineering, Waseda University, Japan. (59-309, 3-4-1 Okubo, Shinjuku Ward, Tokyo, Japan E-mail:hiroki_watanabe@suou.waseda.jp)

N. Yamazaki, Y. Isobe, X. W. Lu, Members of the Graduate School of Science and Engineering, Waseda University, Japan.

T. Ohdaira, M. Hashizume, Members of the Center for the Integration of Advanced Medicine and Innovative Technology, Kyushu University Hospital, Japan.

A. Practical limitations of RF ablation

Although RF ablation is a minimally invasive procedure, it does have some limitations. (1) Imaging modalities such as ultrasonography display only a monochromatic image of the ablation area. (2) The power supply is not optimized for formation of an adequate ablation area. (3) It is not possible to generate an adequate ablation area for large tumors because of the cooling effect of capillary vessels. (4) It is not possible to form a zone for coagulation that conforms to a tumor that is nonspherical. Therefore, it is difficult to control precisely the size and shape of coagulation zones, and this shortcoming may result in tumor recurrence in areas that have not been fully cauterized.

B. Robot-assisted RF ablation

In recent years, considerable research has been undertaken to develop surgical robots and navigation systems for minimally invasive and precise surgery [1], [2], and we recently proposed a robot-assisted RF ablation therapeutic system [3], [4]. This robotic system is based on a precise thermophysical model that predicts in real time the temperature distribution in the organ during RF ablation to calculate and supply the appropriate amount of electrical power to the RF electrode for precise intraoperative surgical control.

C. Thermophysical model of organs

The thermophysical model is constructed from two essential components: a reliable database of the thermophysical properties of the organ (such as specific heat and thermal conductivity) and an accurate temperature distribution simulator based on the finite element method. An accurate simulator must use the appropriate thermophysical properties of the organ. However, creating an accurate model is a challenging problem because of the complexities of the physical properties of the organ.

The thermophysical properties such as the specific heat capacity and the thermal conductivity change with the tissue temperature, and this is a major complicating factor. These properties are included in Pennes' bioheat transfer equation (Eq. 1), which is used to calculate the tissue temperature around the tumor during ablation [5]:

$$\rho c \frac{\partial T}{\partial t} = \lambda \nabla^2 T + \sigma \left| E \right|^2 - \rho \rho_b c_b F (T - T_b) + Q_m \qquad (1)$$

where ρ is the density of the organ [kg/m^3], c is the heat capacity [J/kgK], T is the temperature [°C], λ is the thermal

conductivity [W/mK], σ is the electrical conductivity [S/m], E is the electrical field [V/m], ρ_b is the density of blood, c_b is the heat capacity of blood, F is the blood perfusion coefficient of the organ [m^3/kgs], θ_b is the blood temperature, and Q_m is the metabolic heat source term of the organ [W/m^3].

In fact, work by Webster and by Wolf indicated that the tissue temperature dependence of the thermal conductivity is the phenomenon most likely to affect the accuracy of the temperature distribution simulator for RF ablation [6], [7]. Although some reports have compared the simulated results of the temperature distribution during RF ablation using temperature-dependent and temperature-independent models, there is no report of work evaluating how the accuracy is improved when using the temperature-dependent model with reference to actual temperatures measured in experiments.

The novel aspect of this study is elucidation of the effect of the temperature dependence of the thermal conductivity not only using numerical simulations but also using temperature measurements from in vitro experiments. In this study, we carried out two types of temperature distribution simulations. One adopted the temperature-dependent liver model, which used temperature-dependent values for thermal conductivity. The other adopted the temperature-independent liver model, which used a constant value for thermal conductivity. We evaluated to what extent the accuracy was improved when adopting the temperature-dependent liver model by comparing the simulation results of the two models with the temperature distribution obtained from in vitro experiments on isolated hog liver. We previously measured and reported the temperature dependence of the thermal conductivity of hog liver [3]. In that report, we compared the experimental results for the temperature dependence of the thermal conductivity of hog liver using three different methods to measure the temperature. We confirmed that the results obtained using the unsteady hot wire method were the most reliable because the sample was not deformed during the experiments. Therefore, in Section II of this article, we present a brief explanation of the unsteady hot wire method for obtaining the temperature dependence of the thermal conductivity of hog liver. In Section III, simulations using the temperature-dependent and the temperature-independent models are described. In Section IV, the results of in vitro experiments and the comparison of simulations and experiments are discussed. Finally, in Section V, our conclusions and future work are described.

II. Thermal Conductivity

1) Method: We measured the thermal conductivity of hog liver in the temperature range 10°C to 100°C by the unsteady hot wire method using a QTM-500 quick thermal conductivity meter (Fig. 1: Kyoto Electronics Manufacturing). Measurements were performed on two individual hog livers.

2) Results and discussion: Figure 2 shows the thermal conductivity of hog liver obtained as an average of two trials. According to the results shown in Fig. 2, the thermal conductivity of hog liver rapidly decreased nonlinearly in the

Fig. 1 Experimental setup using a temperature-controlled bath

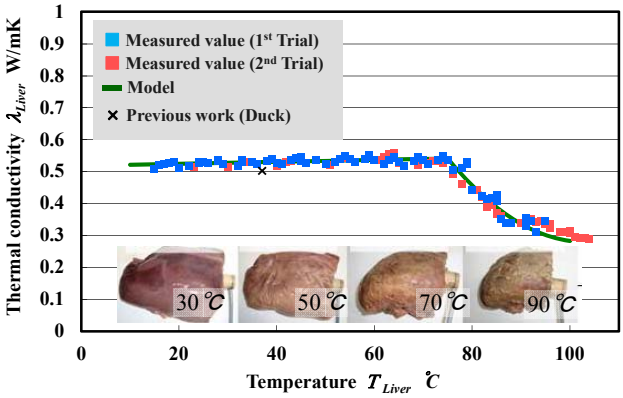

Fig. 2 Experimental results obtained using the unsteady hot wire method

relationship between the temperature T_{Liver} and the thermal conductivity λ_{Liver} was modeled as shown in Eqs. 2 and 3:

$$\lambda_{Liver} = a_1 T_{Liver} + b_1 \qquad (0 \le T_{Liver} \le 75) \tag{2}$$

$$\lambda_{Liver} = a_2 T_{Liver}^{\ 2} + b_2 T_{Liver} + c_2 \qquad (75 \le T_{Liver}) \tag{3}$$

Figure 2 also shows the appearance of hog liver after measurements were taken at the temperatures shown. The volume of hog liver rapidly decreased at temperatures above 70°C following moisture evaporation and protein denaturation. The tendency of the thermal conductivity to increase below 75°C was completely negated in the high temperature range because water in the liver evaporated.

III. Simulation

To investigate the effect of the temperature dependence of the thermophysical properties of liver on the temperature distribution during RF ablation, we evaluated the results from two liver models: (A) a temperature-independent liver model with constant thermal conductivity based on our previous work, and (B) a temperature-dependent liver model with variable thermal conductivity values obtained from the experiments described in Section II. A three-dimensional temperature distribution simulator was developed using the finite element method to compare the results of the two models.

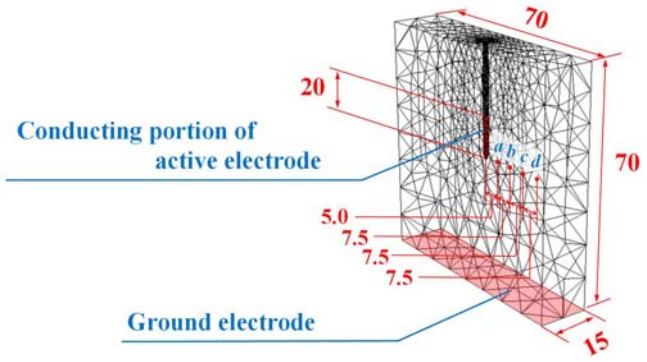

Fig. 3 Simulation model based on the finite element method

Table 1 Electrical and thermal properties

	Model (A)	Model (B)
Density ρ [kg/m^3]	1060	1060
Specific heat c [J/kgK]	3600	3600
Thermal conductivity λ [W/mK]	0.502	Eq. 2, Eq. 3
Electrical conductivity σ [S/m]	0.148	0.148
Blood perfusion coefficient F[m^3/kgs]	0	0

Model A, temperature independent; model B, temperature dependent

A. Simulation conditions

The analytical models were a temperature-independent hog liver model (A) and a temperature-dependent hog liver model (B). Figure 3 displays the finite element liver model used in the simulations. The model encompassed a 70 mm × 70 mm × 15 mm cuboid shape. The RF electrode was considered to be inserted from the top surface of the liver into the center of the model. The numbers of elements and nodes were 30841 and 5776, respectively. Initial and boundary conditions were the same in all models. Simulations were carried out for source voltages of 20, 30, 35, and 40 V applied to the conducting areas (the final 20 mm) of the RF electrode. The nonconducting portions of the electrode were given insulating boundary conditions. At the bottom of each model, an electrical boundary condition of 0 V was applied to simulate the return ground electrode. Electrically insulating boundary conditions were applied for other outer surfaces. An initial thermal condition of 36°C was applied to all elements. The thermal boundary condition for the upper, lower, and side surfaces was 36°C, and for the front and back surfaces was 0 W/m^2. Thermally insulating boundary conditions were applied for the electrode surfaces. These conditions are the same as those used for the in vitro experiments in Section IV.

B. Electrical and thermal properties

The electrical and thermophysical properties used for this simulation are shown in Table 1. The values for the density, specific heat, and electrical conductivity σ for all models were based on the work of Chang [8] and Duck [9]. The thermal conductivity of liver, λ_{Liver}, was determined based on the work of Duck [9] for model A, and on Eqs. 2 and 3 for model B.

C. Results and discussions

Figures 4 and 5 show the simulation results at 5 min and 60 min for models A and B for an electrode source of 30 V. Figure 4 shows no significant differences in temperature between the two liver models around the electrode at 5 min; however, at 60 min, the temperature around the electrode in the temperature-dependent model was higher than that in the temperature-independent model. Figures 6–9 show temperature profiles at points *a–d* for electrode source voltages of 20, 30, 35, and 40 V, respectively. In Figures 6–9, the temperature for each point in the temperature-dependent model is lower than that in the temperature-independent model over almost the entire temperature range. For temperatures below 90°C, the temperature differences between the two models are only a few degrees. However, as shown in Fig. 9, there are large temperature differences at temperatures above 90°C. These features can be explained by differences of the thermal conductivities of the two models. In general, the temperature in a high-thermal-conductivity area remains low because heat input into the area quickly flows into the surrounding areas and does not accumulate. In contrast, the temperature in a low-thermal-conductivity area becomes higher than that in the surrounding areas because heat flows into the surrounding areas slowly and can accumulate. In other words, the temperature at a given point is inversely proportional to the thermal conductivity at that point. As shown in Fig. 2, the thermal conductivities of the two models are approximately equal in the low temperature range, whereas the thermal conductivity of the temperature -dependent model is considerably lower than that of the temperature-independent model at temperatures above 75°C. Therefore, it is considered that the simulated temperatures of the temperature-dependent model become higher than those of the temperature-independent model in the high temperature range because the thermal conductivity is lower.

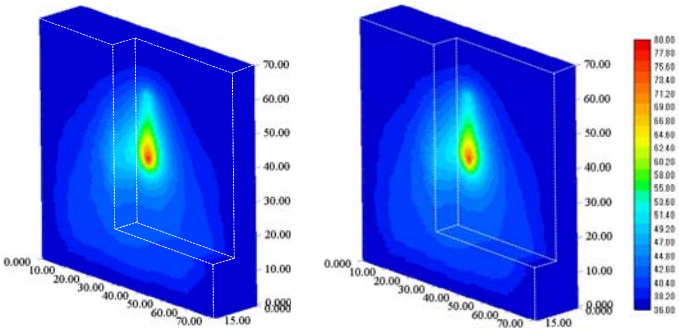

(a) Temperature-independent model (b)Temperature-dependent model

Fig. 4 Simulation result at 5 min (30V)

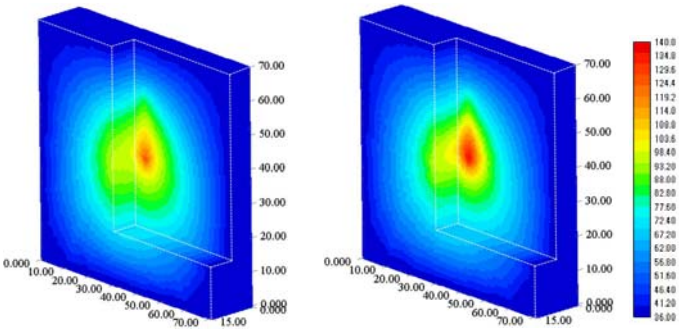

(a) Temperature-independent model (b)Temperature-dependent model

Fig. 5 Simulation result at 60 min (30V)

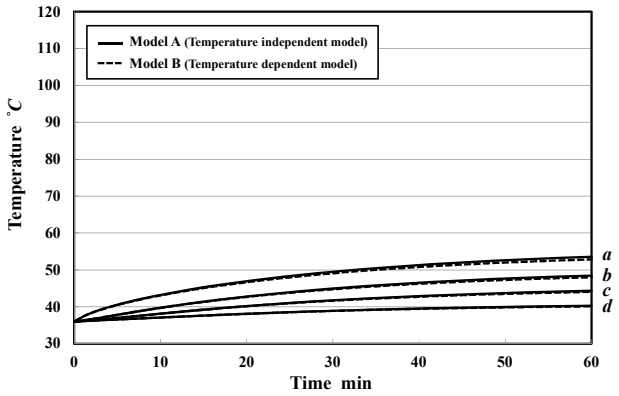

Fig. 6 Temperature profiles with the electrode source at 20 V

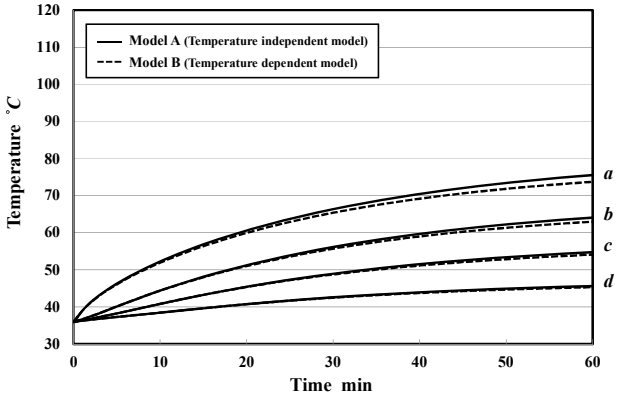

Fig. 7 Temperature profiles with the electrode source at 30 V

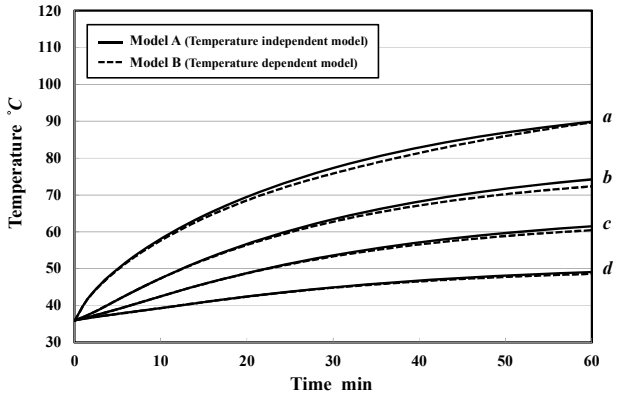

Fig. 8 Temperature profiles with the electrode source at 35 V

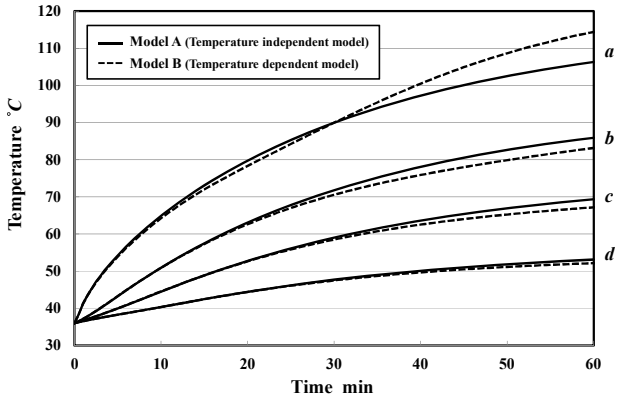

Fig. 9 Temperature profiles with the electrode source at 40 V

IV. Experiment

To evaluate whether the accuracy was improved when the temperature-dependent liver model was used in the simulation, we carried out in vitro ablation experiments using isolated hog liver and compared the temperature distribution based on the simulations and the in vitro experiments.

A. Method

Figure 10 shows the experimental setup with an enlarged view around the experimental liver sample. In this experiment, we ablated isolated hog liver using a Cool-tip RF system under the same physical conditions as those used in the simulations described in Section III. To match the ablation conditions used in the experiments and the simulations, we used a sample holder that could maintain the shape of the sample and control the boundary temperatures. The surfaces of the upper, right, and left sides of the sample holder were formed as a double structure so that hot water could circulate around the sample to control the boundary temperature. The temperature of the hot water was controlled by a temperature-controlled bath. The lower surface of the sample was in contact with a return electrode that was heated to the target boundary temperature by a hot plate. Moreover, the front and the back surface of the sample were thermally insulated by the surrounding air. There were four holes in the front surface of the sample holder to allow the thermocouples to be inserted into the center of the sample, and there was one hole in the upper surface to allow insertion of a needle type active electrode into the center of the sample. The return electrode on the lower side absorbed the RF current flowing from the active electrode. Using these devices, we carried out ablation experiments as follows: 1) First, the hog liver was cut into samples 70 mm × 70 mm × 15 mm, and the samples were set in the sample holder. 2) The temperature of the liver was controlled at 36°C by hot water flowing around the circumference of the liver and the hot plate. 3) After the temperature of the liver reached the target temperature, the needle type active electrode and the four thermocouples were inserted into the liver. 4) Voltages of 20, 30, 35, and 40 V were applied to the liver from the active electrode, and the temperature at points *a–d* were measured during ablation.

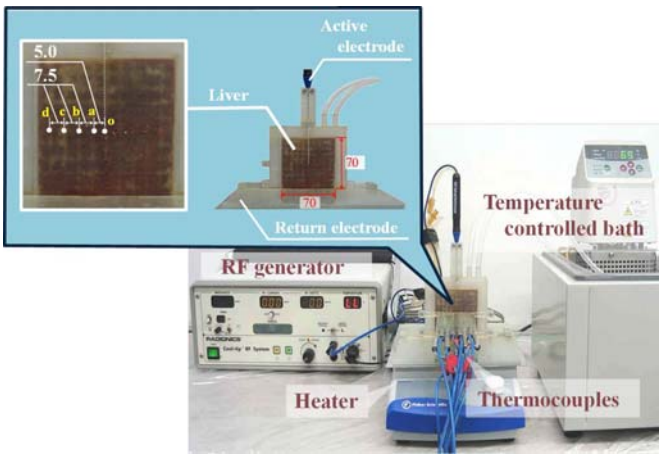

Fig. 10 In vitro experimental setup

B. Results and discussions

Figures 11–14 show the experimental results at each voltage. And Fig. 15 shows the appearance of ablated liver and liver model at 10 min at 30 V. In figures 11-14, the simulated temperatures of the temperature-independent model and the temperature-dependent model are also shown. As shown in Figs. 13 and 14 (electrode at 35 V and 40V), the liver could not continue to be ablated after the temperature at point *a* reached 80°C because the tissue surrounding the electrode was burned as a result of the rapid temperature rise. During ablation at 35 V and 40 V, the temperature of the tissue surrounding the electrode was assumed also to have reached about 90°C when the temperature at point *a* reached 90°C (the distance between the electrode and point *a* was 5 mm.) Heat generation was automatically stopped and the temperature at each point decreased as soon as the temperature of the electrode reached about 90°C. Therefore, we could not compare the measured temperatures and simulated values at high temperatures. For electrode temperatures up to about 80°C, the following two features are apparent in the results:

1) The accuracy of the simulation at points far from the electrode (points *c* and *d*) is lower than that at points closer to the electrode (points *a* and *b*).

2) There is no significant improvement of simulation accuracy when using the temperature-dependent model compared with the temperature-independent model.

With respect to item 1), the low simulation accuracy at points far from the electrode was likely caused by the inaccurate experimental reflection of the thermal boundary conditions used in the simulations. During the ablation experiments, there was the possibility that the temperature around the liver sample varied irregularly by location. Therefore, it is considered that there were some differences in boundary temperature between the simulation liver model and the experimental liver sample. With respect to item 2), there was no major difference in simulation accuracy between the temperature-independent model and the temperature -dependent model for all voltages considered. As mentioned in Section III, this is because the difference in predicted temperatures in the two models is only a few degrees within the low temperature range. In theory, although a major improvement in accuracy might have occurred at high temperatures when using the temperature-dependent model (because there are large differences in thermal conductivity values between the two models at high temperature), it was not possible to confirm this because the heat generation was stopped after the temperature of the tissue surrounding the electrode reached about 90°C, and therefore high temperatures were not attained. In practical RF ablation, very high temperatures do not occur because the tissue surrounding the electrode is carbonized and the RF current is interrupted. This means that high temperature areas that could generate large differences in thermal conductivity between the two models do not arise in practice. Consequently, it can be concluded that inclusion of the temperature dependence of thermal conductivity in the simulation does not result in a major increase in simulation accuracy for the conditions prevailing during clinical RF ablation.

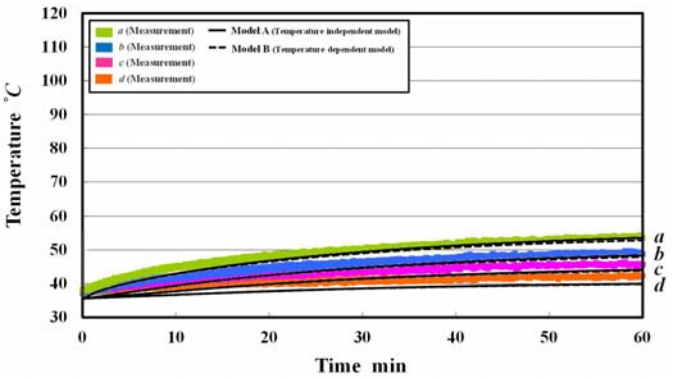

Fig. 11 Comparison of simulated temperature and measured temperature at 20 V

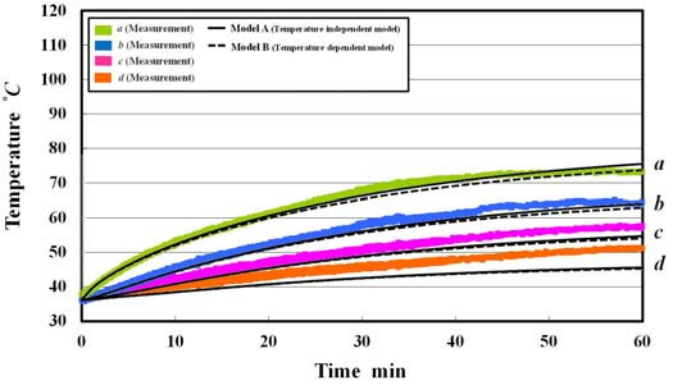

Fig. 12 Comparison of simulated temperature and measured temperature at 30 V

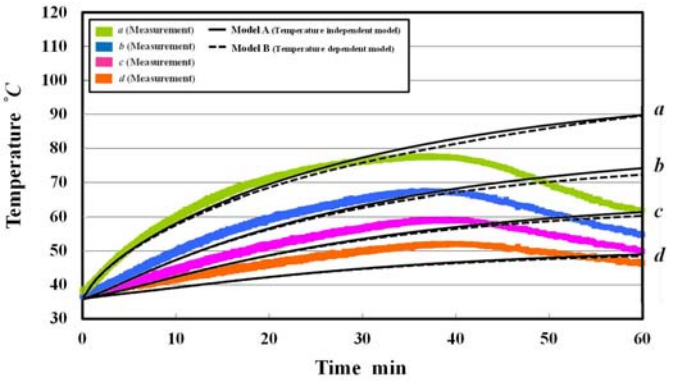

Fig. 13 Comparison of simulated temperature and measured temperature at 35 V

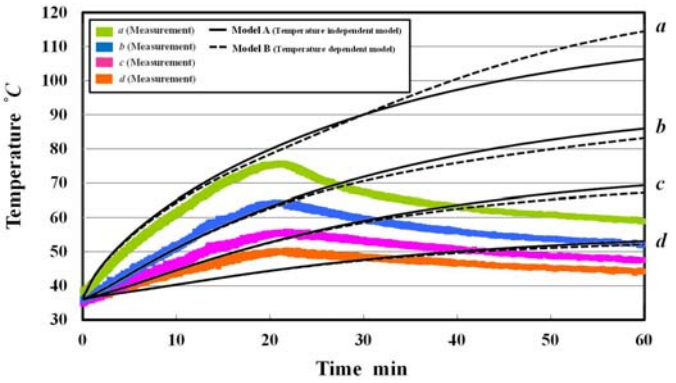

Fig. 14 Comparison of simulated temperature and measured temperature at 40 V

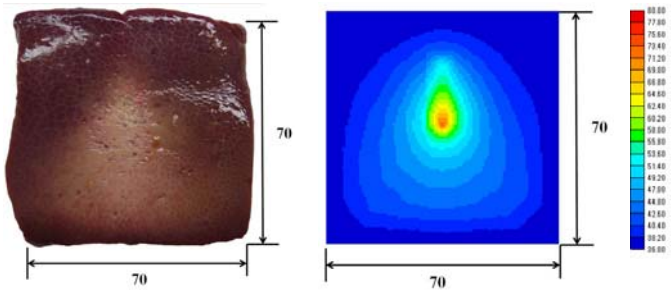

(a) Ablated liver in vitro experiment (b) Liver model in the simulation

Fig. 15 Comparison of appearance between actual liver and model at 10 min at 30V

V. CONCLUSION AND FUTURE WORK

In this article, we evaluated the improved accuracy of the temperature-dependent liver model by comparing the simulated temperatures with the results of in vitro experiments using hog liver. First, the experiment to obtain the temperature dependence of the thermal conductivity of hog liver was described. Then, we evaluated the differences in the simulation results between the temperature-independent liver model and the temperature-dependent liver model in a finite element simulation. Finally, in vitro experiments were carried out to evaluate the improvement in accuracy obtained when adopting the temperature-dependent liver model. By comparison with the experimental results, it was confirmed that there was no major improvement in simulation accuracy when adopting the temperature-dependent model because the high temperature areas that could generate large differences in simulation results between the two models do not appear during practical RF ablation. The reason that such high temperatures do not occur is that tissue surrounding the electrode is carbonized and the RF current is interrupted.

In the future, we will carry out in vivo experiments using living animals to establish whether the differences in the accuracy of the temperature-independent model and the temperature-dependent model are significant under actual RF ablation conditions in which the liver has blood flowing through it. Moreover, organ model-based ablation systems will be further developed to achieve safe and precise clinical RF ablation treatments.

REFERENCES

[1] R. H. Taylor and D. Stoianovici, "Medical Robotics in Computer-Integrated Surgery", IEEE Transactions on Robotics and Automation, Vol. 19, No. 5, pp. 765-781, 2003.

[2] P. Daraio, B. Hannaford and A. Menciassi, "Smart Surgical Tools and Augmenting Devices", IEEE Transactions on Robotics and Automation, Vol. 19, No. 5, pp. 782-792, 2003.

[3] H. Watanabe, N. Yamazaki , Y. Kobayashi, T. Miyashita, M. Hashizume, M. G. Fujie, "Temperature Dependence of Thermal Conductivity of Liver Based on Various Experiments and a Numerical Simulation for RF Ablation", in Proceeding of the 32nd Annual International Conference of the IEEE Engineering in Medicine and Biology Society, pp. 3222-3228, 2010.

[4] H. Watanabe, N. Yamazaki, Y. Kobayashi, T. Miyashita, M. Hashizume, M. G. Fujie, "Estimation of Intraoperative Blood Flow During Liver RF Ablation Using a Finite Element Method-based Biomechanical Simulation", in Proceeding of the 33rd Annual International Conference of the IEEE Engineering in Medicine and Biology Society (EMBC'11), pp.7441-7445, 2011.

[5] H. H. Pennes, "Analysis of Tissue and Arterial Blood Temperatures in the Resting Human Forearm", Journal of Applied Physiology, Vol. 1, No. 2, pp. 93-122, 1948.

[6] D. Haemmerich, S. Tungjitkusolmun, S. T. Staelin, F. T. Lee, Jr., D. M. Mahvi, J. G. Webster, "Finite-Element Analysis of Hepatic Multiple Probe Radio-Frequency Ablation", IEEE Transactions on Biomedical Engineering, Vol. 49, No. 7, pp. 836-842, 2002.

[7] M. K. Jain, P. D. Wolf, "A Three-Dimensional Finite Element Model of Radiofrequency Ablation with Blood Flow and its Experimental Validation", Annals of Biomedical Engineering, Vol. 28, pp. 1075-1084, 2000.

[8] I. Chang, "Finite Element Analysis of Hepatic Radiofrequency Ablation Probes Using Temperature-Dependent Electrical Conductivity", Biomedical Engineering Online, 2:12, 2003.

[9] Duck F, "Physical Properties of Tissue", A Comprehensive Reference Book, Academic Press, pp. 167-223, New York 1998.